

# PEP-GS: Perceptually-Enhanced Precise Structured 3D Gaussians for View-Adaptive Rendering

Junxi Jin<sup>1</sup>, Xiulai Li<sup>1\*</sup>, Haiping Huang<sup>1</sup>, Lianjun Liu<sup>1</sup>,  
Yujie Sun<sup>1</sup> and Logan LIU<sup>2</sup>

<sup>1</sup>Hainan University, Haikou, China

<sup>2</sup>The Hong Kong University of Science and Technology, Hong Kong SAR  
{junxijin, lixiulai01, huanghp, lianjun\_320, sunyujie}@hainanu.edu.cn  
bliubd@connect.ust.hk

## Abstract

Recently, 3D Gaussian Splatting (3D-GS) has achieved significant success in real-time, high-quality 3D scene rendering. However, it faces several challenges, including Gaussian redundancy, limited ability to capture view-dependent effects, and difficulties in handling complex lighting and specular reflections. Additionally, methods that use spherical harmonics for color representation often struggle to effectively capture anisotropic components, especially when modeling view-dependent colors under complex lighting conditions, leading to insufficient contrast and unnatural color saturation. To address these limitations, we introduce PEP-GS, a perceptually-enhanced framework that dynamically predicts Gaussian attributes, including opacity, color, and covariance. We replace traditional spherical harmonics with a Hierarchical Granular-Structural Attention mechanism, which enables more accurate modeling of complex view-dependent color effects. By employing a stable and interpretable framework for opacity and covariance estimation, PEP-GS avoids the removal of essential Gaussians prematurely, ensuring a more accurate scene representation. Furthermore, perceptual optimization is applied to the final rendered images, enhancing perceptual consistency across different views and ensuring high-quality renderings with improved texture fidelity and fine-scale detail preservation. Experimental results demonstrate that PEP-GS outperforms state-of-the-art methods, particularly in challenging scenarios involving view-dependent effects and fine-scale details.

## 1 Introduction

The rendering of 3D scenes has long been a cornerstone of both computer vision and graphics research, with numerous applications across industries such as virtual reality [Jiang *et al.*, 2024a; Xie *et al.*, 2024; Xu *et al.*, 2023], autonomous driving [Zhou *et al.*, 2024; Jiang *et al.*, 2024b], and drivable human avatars [Qian *et al.*, 2024b; Qian *et al.*, 2024a;

\*Corresponding Author

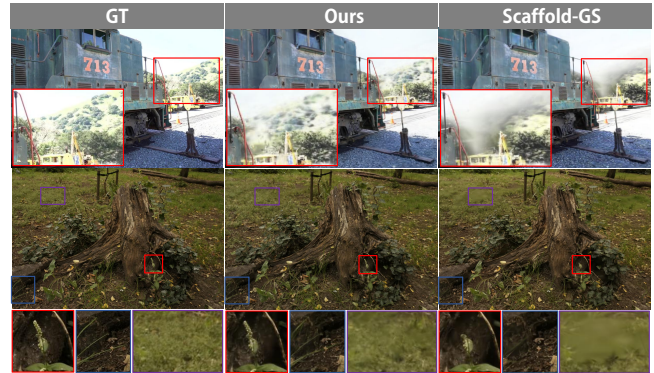


Figure 1: Comparison of PEP-GS against SOTA methods. Our method achieves better perceptual consistency and more accurate view-dependent effects across different viewing angles, particularly in scenes with complex lighting and textures

Zheng *et al.*, 2024]. Traditional methods, such as meshes and point clouds [Botsch *et al.*, 2005; Munkberg *et al.*, 2022; Yifan *et al.*, 2019], are efficient but often compromise visual quality, leading to discontinuities. In contrast, volumetric representations like Neural Radiance Fields (NeRF) [Barron *et al.*, 2022; Mildenhall *et al.*, 2021; Barron *et al.*, 2023] deliver photorealistic results but are computationally intensive, particularly for real-time rendering. Recently, 3D Gaussian Splatting (3D-GS) [Kerbl *et al.*, 2023] has emerged as a promising solution, enabling high-quality, real-time rendering of scenes using 3D Gaussian primitives, thus bypassing the need for complex ray-sampling techniques.

Although 3D-GS demonstrates impressive rendering performance, it struggles with capturing complex view-dependent effects, especially in dynamic lighting environments. This limitation stems from the inherent constraints of low-order spherical harmonics (SH) used for color representation in 3D-GS, which are well-suited for modeling subtle, view-dependent phenomena but struggle to accurately represent anisotropic components. Due to their low-frequency nature, SH functions struggle to capture high-frequency, view-dependent details under dynamic lighting, which limits their effectiveness in complex scenes. Moreover, structured approaches like Scaffold-GS reduce Gaussian redundancy through hierarchical and region-aware scene representation but struggle with fine-scale details and texture mod-

eling, leading to perceptual inconsistencies under complex lighting and reflections.

To address these challenges, we propose PEP-GS, a perceptually-enhanced framework for structured 3D Gaussian splatting inspired by previous work [Lu *et al.*, 2024; Laparra *et al.*, 2016; Xu and Wan, 2024]. Similarly, we construct a sparse grid of anchor points, initialized from SfM points. For each neural Gaussian tethered to these anchors, PEP-GS dynamically predicts Gaussian attributes including opacity for transparency control, color for view-dependent appearance modeling, and covariance for spatial representation using a stable and precise framework. Specifically, we replace the traditional SH-based color representation with a Hierarchical Granular-Structural Attention mechanism, enabling more accurate modeling of view-dependent color effects. Additionally, we integrate Kolmogorov-Arnold Networks (KAN) for opacity and covariance estimation, enhancing the stability of the predictions. Building on this, we apply perceptual optimization techniques to improve the consistency of the rendered results. This approach refines the image details and texture fidelity, optimizing visual consistency across different views and significantly improving perceptual fidelity and fine-scale detail preservation in the final rendered images.

Through extensive experimentation, we demonstrate that our approach significantly outperforms existing state-of-the-art methods. As shown in Figure. 1, it shows particular strength in handling challenging scenarios such as view-dependent lighting effects, and intricate geometric details. Notably, our method maintains stability and consistently improves visual quality and perceptual consistency across novel views.

The primary contributions of this work are:

- A perceptually-enhanced framework for structured 3D Gaussian splatting that significantly improves rendering quality in view-dependent scenarios while avoiding the premature removal of essential neural Gaussians, ensuring efficient scene representation.
- Novel neural architectures that effectively and stably predict key Gaussian attributes, addressing critical limitations in current Gaussian-based rendering approaches, particularly in terms of accuracy and stability under complex lighting conditions.
- Comprehensive experimental validation demonstrating substantial improvements in rendering quality across multiple datasets, particularly in challenging scenarios involving complex lighting and fine geometric details.

## 2 Related work

### 2.1 Neural Scene Representations and 3D Gaussians

Neural scene representation has evolved significantly from early MLP-based approaches to current state-of-the-art methods. NeRF [Mildenhall *et al.*, 2021] pioneered the use of volumetric representations through coordinate-based neural networks, achieving high-quality results but suffering from slow rendering speeds. Subsequent works explored various

acceleration techniques [Cao *et al.*, 2023; Chen *et al.*, 2022; Chen *et al.*, 2023; Reiser *et al.*, 2021; Reiser *et al.*, 2023; Sitzmann *et al.*, 2021]. Although NeRF-based methods have made significant strides in volumetric rendering, achieving an optimal balance between visual fidelity and processing speed remains a major challenge. Meanwhile, point-based rasterization [Franke *et al.*, 2023; Franke *et al.*, 2024; Kopanas *et al.*, 2021; Xu *et al.*, 2022] approaches have attracted attention for their ability to deliver competitive rendering performance with improved computational efficiency. A breakthrough came with 3D Gaussian Splatting (3D-GS) [Kerbl *et al.*, 2023], which achieves real-time performance by explicitly modeling the scene with optimized 3D Gaussians and a differentiable rasterization pipeline. However, this can result in redundant Gaussians that attempt to fit every training view, negatively impacting robustness under significant view changes and challenging lighting conditions. The Scaffold-GS [Lu *et al.*, 2024] subsequently introduced a structured hierarchy of 3D Gaussians anchored by sparse SfM [Snively *et al.*, 2023] points, effectively reducing redundant Gaussian usage and enhancing the representation’s adaptability to varying levels-of-detail.

### 2.2 View-dependent Appearance Modeling

Accurately capturing high-frequency view-dependent phenomena (e.g., specular reflections) remains a key challenge in neural rendering. Existing volumetric methods, including NeRF derivatives, often rely on explicit or implicit encodings to handle view dependence [Xu *et al.*, 2022; Barron *et al.*, 2022; Müller *et al.*, 2022] but can struggle with glossy materials and realistic reflectance. In the 3D-GS family, spherical harmonics (SH) have been widely adopted for their computational efficiency [Kerbl *et al.*, 2023; Fridovich-Keil *et al.*, 2022], yet they primarily excel at modeling subtle view-dependent effects and can introduce artifacts for complex lighting. Several approaches have attempted to overcome these limitations through various encoding schemes [Verbin *et al.*, 2022; Ma *et al.*, 2024; Yang *et al.*, 2024]; however, achieving perceptual consistency across different viewing angles while preserving geometric details remains challenging. Our work addresses these limitations through a perceptually-enhanced framework that better handles view-dependent effects and geometric details while maintaining rendering consistency across different views.

## 3 Methodology

The overview of our method is illustrated in Figure. 2 Starting with anchor points derived from SfM data, each anchor encodes localized scene information to guide tethered neural Gaussians, which dynamically predict attributes such as opacity, color, rotation, and scale based on the viewing angle. To improve the modeling of view-dependent lighting effects, we replace spherical harmonics with Hierarchical Granular-Structural Attention Mechanism to predict the color attribute, which enables more effective capture of local geometric features and complex view-dependent color changes. For opacity, rotation, and scale, we employ Kolmogorov-Arnold Networks [Liu *et al.*, 2024], offering a more interpretable and precise framework for neural Gaussian attribute

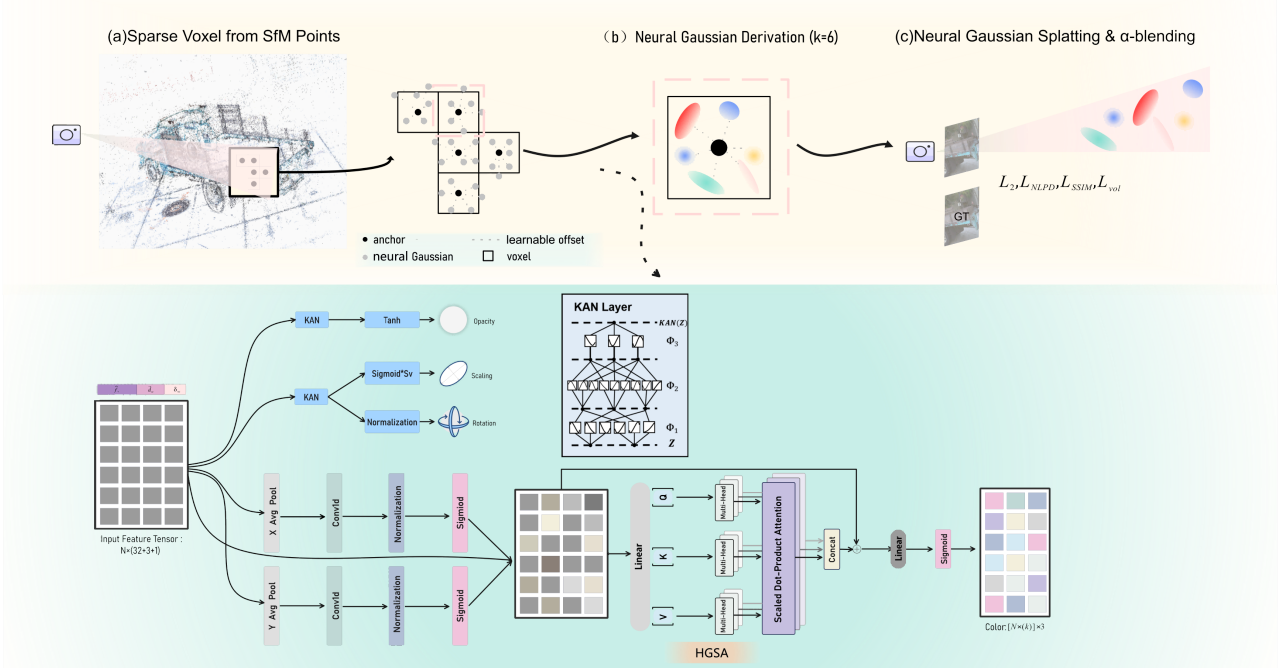


Figure 2: Overview of PEP-GS

prediction. Finally, we incorporate the Normalized Laplacian Pyramid Distance ( $L_{NLPD}$ ) as a perceptual loss function to ensure cross-view perceptual consistency, resulting in coherent, high-quality renderings.

### 3.1 Preliminaries

3D Gaussian Splatting [Kerbl *et al.*, 2023] (3D-GS) models scenes using a collection of anisotropic 3D Gaussians, each defined by center position  $\mu$ , opacity  $\alpha$ , covariance matrix  $\Sigma$ , and spherical harmonic (SH) coefficients. Specifically, each 3D Gaussian is centered at  $\mu$  with a covariance  $\Sigma$ :

$$G(x) = e^{-\frac{1}{2}(x-\mu_i)^T \Sigma_i^{-1}(x-\mu_i)}, \quad (1)$$

where  $x$  is an arbitrary position within the 3D scene. The positive semi-definite covariance matrix  $\Sigma$  is constructed from scaling  $S$  and rotation  $R$  matrices as  $\Sigma = RSS^T R^T$ . Then 3D Gaussians  $G$  are projected to 2D Gaussians  $G'$  for rendering. Using depth-sorted 2D Gaussians, the tile-based rasterizer applies  $\alpha$ -blending to calculate pixel color  $C(x')$ :

$$C(x') = \sum_{i=1}^N c_i \alpha_i G_i(x') \prod_{j=1}^{i-1} (1 - \alpha_j G_j'(x')), \quad (2)$$

where  $N$  is the count of Gaussians overlapping the pixel, and  $c_i$  is the color from SH coefficients. Gaussians are adaptively adjusted during optimization for accurate scene representation. For details, see [Kerbl *et al.*, 2023].

Scaffold-GS [Lu *et al.*, 2024] extends 3D-GS by introducing a structured and sparse hierarchical representation initialized from a COLMAP point cloud  $\mathbf{P} \in \mathbb{R}^{M \times 3}$ . The points are voxelized into anchors:

$$\mathbf{V} = \left\{ \left\lfloor \frac{\mathbf{P}}{\epsilon} \right\rfloor \right\} \cdot \epsilon, \quad (3)$$

where  $\epsilon$  is the voxel size. Each anchor  $v \in \mathbf{V}$  is characterized by a feature  $f_v$ , a scale  $l_v$ , and  $k$  learnable offsets  $\mathbf{O}_v$ . To achieve multi-resolution and view-dependent modeling, a feature bank  $\{f_v, f_{v_{\downarrow 1}}, f_{v_{\downarrow 2}}\}$  is constructed, consisting of the original anchor feature and two downsampled versions at different levels. For a given camera position  $\mathbf{x}_c$ , the distance  $\delta_{vc}$  and direction  $\bar{\mathbf{d}}_{vc}$  between the anchor and the camera are computed, where  $\delta_{vc}$  represents the Euclidean distance between the anchor and the camera, and  $\bar{\mathbf{d}}_{vc}$  is the normalized displacement vector indicating the viewing direction from the camera to the anchor. These spatial relationships are then processed through a multi-layer perceptron (MLP), which predicts the blending weights  $\{w, w_1, w_2\}$ . The weights are normalized using the softmax function and are applied to the feature bank to obtain the final blended feature  $\hat{f}_v$  as follows:

$$\hat{f}_v = w \cdot f_v + w_1 \cdot f_{v_{\downarrow 1}} + w_2 \cdot f_{v_{\downarrow 2}} \quad (4)$$

This structured approach dynamically refines the attributes of Gaussians during training to better capture scene geometry and view-dependent details while reducing redundancy and maintaining high rendering quality.

### 3.2 PEP-GS

#### View-Adaptive Color Refinement with Attention Mechanisms

To capture complex view-dependent appearance changes under varying lighting and viewing conditions, we propose Hierarchical Granular-Structural Attention (HGSA), which integrates fine-grained feature enhancement and structural-level attention to dynamically aggregate features. This hierarchical mechanism adapts to directional changes and effectively combines detail-sensitive and global context information to optimize color representation.

Given an input feature  $\mathbf{f}_{in} \in \mathbb{R}^{N \times (32+3+1)}$ , which is formed by concatenating the viewing direction  $\delta_{vc}$ , the relative distance  $\vec{\mathbf{d}}_{vc}$ , and the integrated anchor feature  $\hat{\mathbf{f}}_v$ :

$$\mathbf{f}_{in} = \delta_{vc} \oplus \vec{\mathbf{d}}_{vc} \oplus \hat{\mathbf{f}}_v, \quad (5)$$

where  $\oplus$  denotes the operation of concatenation. As shown in Eq. 6, we first apply average pooling separately along two directions: horizontally (along the height) and vertically (along the width). These pooled features are then processed through a 1D convolutional layer, followed by a custom normalization and a sigmoid activation function to generate positional attention maps in both directions  $y^h$  and  $y^w$ .

$$z^h(h) = \frac{1}{H} \sum_{0 \leq i < H} \mathbf{f}_{in}(h, i), \quad z^w(w) = \frac{1}{W} \sum_{0 \leq j < W} \mathbf{f}_{in}(j, w). \quad (6)$$

where the input feature  $\mathbf{f}_{in}$  is a concatenation of three tensors: the anchor feature  $\hat{\mathbf{f}}_v$ , the relative viewing distance  $\delta_{vc}$ , and the direction  $\vec{\mathbf{d}}_{vc}$  between the camera and the anchor point. These attention maps are then multiplied element-wise with the original input feature tensor  $\mathbf{f}_{in}$ , yielding refined granular regional feature  $\mathbf{f}_{gra}$ .

$$\mathbf{f}_{gra} = \mathbf{f}_{in} \times y^h \times y^w, \quad (7)$$

Next, we apply structural-level attention to capture global dependencies and encode structural relationships across the input feature space. This attention mechanism uses a multi-head attention framework, where the granular regional feature  $\mathbf{f}_{gra}$  is first projected into query  $Q$ , key  $K$ , and value  $V$  spaces using learnable weight matrices. The attention mechanism computes contextual relevance between features by applying the scaled dot-product attention, and the resulting attention weights are used to aggregate the global context into the output feature  $\mathbf{O}$ :

$$\mathbf{O} = \text{Softmax} \left( \frac{QK^T}{\sqrt{d_{\text{head}}}} \right) V, \quad (8)$$

The multi-head outputs are concatenated and projected back to the original input dimension. To ensure stability, residual connections and LayerNorm are applied:

$$\mathbf{f}_{\text{HGSA}} = \text{LayerNorm}(\mathbf{O} + \mathbf{f}_{gra}). \quad (9)$$

The structural-level attention mechanism plays a pivotal role in encoding global dependencies, allowing the model to capture long-range interactions and maintain structural consistency across the feature space. By aggregating context-aware information, it complements the granular component, resulting in a unified representation that effectively integrates fine-grained details with global structure. This integration enables robust optimization of view-dependent color refinement in complex 3D scenes, particularly in scenarios with intricate lighting and occlusions.

## Robust Framework for Gaussian Attribute Estimation

The traditional multilayer perceptron (MLP) is a cornerstone in deep learning, widely used for approximating multivariable functions through a series of nonlinear mappings. An MLP consists of weight matrices  $W$  and activation functions  $\sigma$  applied in alternation, formally expressed as:

$$\text{MLP}(Z) = (W_{K-1} \circ \sigma \circ W_{K-2} \circ \sigma \circ \dots \circ W_1 \circ \sigma \circ W_0)Z, \quad (10)$$

where  $Z$  is the input,  $W_i$  are weight matrices, and  $\sigma$  denotes activation functions. Despite its versatility, the application of MLPs in high-fidelity 3D reconstruction tasks is hindered by their computational complexity and inability to handle high-dimensional features effectively. This limits their capacity to model intricate geometries, fine-scale textures, and subtle color variations, leading to issues such as shadow artifacts, loss of structural consistency in thin geometries, and suboptimal color rendering in challenging lighting conditions.

In contrast, the Kolmogorov-Arnold Network (KAN), grounded in the Kolmogorov-Arnold representation theorem, introduces a modular and interpretable alternative. Unlike traditional MLPs with fixed activation functions, KAN utilizes learnable activation functions, enhancing the network's adaptability. A  $K$ -layer KAN network is defined as a nested composition of learnable activation layers:

$$\text{KAN}(\mathbf{Z}) = (\Phi_{K-1} \circ \Phi_{K-2} \circ \dots \circ \Phi_1 \circ \Phi_0) \mathbf{Z}, \quad (11)$$

where each layer  $\Phi_i$  contains  $n_{\text{in}} \times n_{\text{out}}$  learnable activation functions  $\phi$ , as shown below:

$$\Phi = \{\phi_{k,q,p}\}, \quad p = 1, 2, \dots, n_{\text{in}}, \quad q = 1, 2, \dots, n_{\text{out}}. \quad (12)$$

The pre-activation of  $\phi_{k,q,p}$  is  $Z_{k,p}$ , while its post-activation is given by:

$$\tilde{Z}_{k,q,p} = \phi_{k,q,p}(Z_{k,p}). \quad (13)$$

The activation value of the  $(k+1, q)$ -th neuron is computed as:

$$Z_{k+1,q} = \sum_{p=1}^{n_k} \tilde{Z}_{k,q,p} = \sum_{p=1}^{n_k} \phi_{k,q,p}(Z_{k,p}), \quad q = 1, \dots, n_{\text{out}}. \quad (14)$$

Building on this foundation, KAN replaces traditional MLPs for processing input feature  $\mathbf{f}_{in}$ . For opacity prediction, a Tanh activation function is applied to the KAN output, with thresholds set to retain essential neural Gaussian distributions ( $\alpha \geq \tau_\alpha$ ) while preventing premature removal of critical components. KAN dynamically adjusts the scale of each neural Gaussian distribution based on anchor features, viewing angle, and position, preserving fine-scale textures and thin geometries. Similarly, KAN predicts rotation parameters, allowing neural Gaussian distributions to adapt their orientation based on the viewing angle, enhancing the capture of spatial relationships and view-dependent occlusions.

KAN's ability to precisely control opacity, scaling, and rotation significantly improves reconstruction quality, ensuring better preservation of intricate textures, thin structures, and fine details. By addressing the limitations of traditional MLPs and Gaussian-based methods, KAN enhances stability and adaptability in view-dependent scenarios, particularly in handling complex lighting, weak textures, and dynamic occlusions.

## Loss Fuction

Our overall loss function is designed as:

$$\mathcal{L} = ((1 - \lambda_{D-SSIM}) \cdot \mathcal{L}_2 + \lambda_{D-SSIM} \cdot \mathcal{L}_{D-SSIM} + \lambda_{vol} \cdot \mathcal{L}_{vol}) \cdot (1 - \lambda_{NLPD}) + \lambda_{NLPD} \cdot \mathcal{L}_{NLPD}, \quad (15)$$

To regulate the volume of neural Gaussians, the regularization term is defined as  $\mathcal{L}_{vol} = \sum_{i=1}^{N_{ng}} \text{Prod}(s_i)$ , where  $N_{ng}$  indicates the total count of neural Gaussians in the scene, and  $\text{Prod}(\cdot)$  calculates the product of the components of a vector, specifically the scale  $s_i$  for each Gaussian in this scenario. In particular,  $\mathcal{L}_{NLPD}$  plays a critical role in maintaining multi-scale perceptual consistency.

The Normalized Laplacian Pyramid Distance (NLPD) loss  $\mathcal{L}_{NLPD}$  is designed to measure multi-scale perceptual differences between the rendered image and the ground truth by leveraging a Laplacian pyramid decomposition to create a multi-resolution representation. At each scale  $i$ , the residual  $R_i$  is computed as the difference between the original image and its reconstructed version. These residuals are then normalized using divisive normalization:

$$R_i^{\text{norm}} = \frac{R_i}{\sigma_i + F(R_i)} \quad (16)$$

where  $\sigma_i$  is a scale-dependent noise parameter, and  $F(\cdot)$  is a local filter applied to the residual magnitudes, ensuring robustness to variations in texture and noise.

The final perceptual difference is obtained by aggregating the squared differences of the normalized residuals between the rendered image and the ground truth across all scales:

$$\mathcal{L}_{NLPD} = \frac{1}{k} \sum_{i=1}^k \sqrt{\frac{1}{N_i} \sum_{j=1}^{N_i} (R_i^{x,\text{norm}}[j] - R_i^{y,\text{norm}}[j])^2} \quad (17)$$

where  $N_i$  represents the number of pixels at scale  $i$ , and  $k$  is the total number of scales considered.

This perceptual loss effectively captures fine-grained details and texture differences across multiple resolutions, enhancing both global structural similarity and local detail consistency. When integrated with other loss components,  $\mathcal{L}_{NLPD}$  ensures perceptually consistent renderings that closely align with the ground truth, even in challenging scenarios involving intricate textures and lighting effects.

## 4 Experiments

### 4.1 Setups

#### Datasets and Metrics

We conduct a comprehensive evaluation of our proposed model on seven scenes from Mip-NeRF360 [Barron *et al.*, 2022], two scenes from Tanks&Temples [Knapitsch *et al.*, 2017], two scenes from DeepBlending [Hedman *et al.*, 2018]. Consistent with methodologies outlined in previous works [Barron *et al.*, 2022; Kerbl *et al.*, 2023], we adopted a train/test split approach where every 8th photo was selected for testing. To assess the rendering quality, we further measured the average Peak Signal-to-Noise Ratio

(PSNR), Structural Similarity Index Measure (SSIM) [Wang *et al.*, 2004], and Learned Perceptual Image Patch Similarity (LPIPS) [Zhang *et al.*, 2018].

#### Implementation Details

To maintain fairness in evaluation, we configure  $k = 10$  for all experiments, consistent with the settings used in Scaffold-GS. In the design of the loss function, we assign a value of 0.2 to  $\lambda_{NLPD}$ . For the HGSA, the multi-head attention mechanism is configured with 7 heads. We assess the quality of our approach by comparing it to current state-of-the-art(SOTA) baselines, including Instant-NGP [Müller *et al.*, 2022], Plenoxels [Fridovich-Keil *et al.*, 2022], Mip-NeRF360 [Barron *et al.*, 2022], 3D-GS, Mip-splatting [Yu *et al.*, 2023] and Scaffold-GS. In line with the approach described in 3D-GS, our models undergo training for 30K iterations across all scenes.

## 4.2 Comparisons

### Quantitative Comparisons.

Table. 1 presents the results on three real-world datasets [Barron *et al.*, 2022; Knapitsch *et al.*, 2017; Hedman *et al.*, 2018], highlighting that our approach achieves competitive performance in rendering quality compared to state-of-the-art methods and stands out in terms of image quality and perceived similarity. While Scaffold-GS achieves the highest PSNR performance on the Deep Blending dataset, our method demonstrates more consistent and robust performance across other datasets, with PEP-GS notably outperforming Scaffold-GS on the Tanks&Temples dataset, as illustrated in Figure. 3. It can be noticed that our approach achieves comparable results with 3D-GS on Mip-NeRF360 dataset, and achieves superior results in Tanks&Temples datasets, exhibiting notable competitiveness in terms of SSIM and LPIPS.

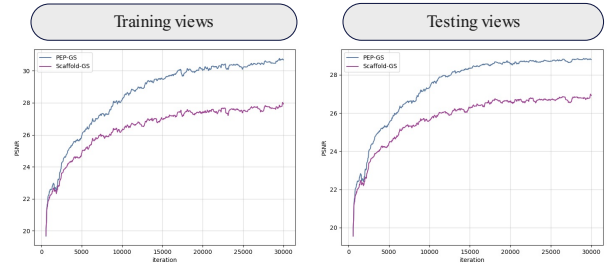


Figure 3: The PSNR curve of Scaffold-GS and PEP-GS across the truck scene in the Tanks & Temples dataset under training and test views.

### Qualitative Comparisons.

Qualitative results across various datasets are provided in Figure. 4. We also conducted a more comprehensive and detailed comparison of rendering results against the scaffold method. As shown in the first and second rows of the left column in Figure. 6, it is evident that our method demonstrates sharper details and textures, effectively preserving local structures and fine-scale details during image reconstruction. As shown in the first and second rows of the right column in Figure. 6, under challenging sunlight environments,

Table 1: Quantitative comparison to previous methods on real-world datasets. Competing metrics are extracted from respective papers.

Dataset		Mipnerf-360			Tanks&Templates			Deep Blending		
Method	Metrics	PSNR $\uparrow$	SSIM $\uparrow$	LPIPS $\downarrow$	PSNR $\uparrow$	SSIM $\uparrow$	LPIPS $\downarrow$	PSNR $\uparrow$	SSIM $\uparrow$	LPIPS $\downarrow$
Instant-NGP		26.43	0.725	0.339	21.72	0.723	0.330	23.62	0.797	0.423
Plenoxels		23.62	0.670	0.443	21.08	0.719	0.379	23.06	0.795	0.510
Mip-NeRF360		29.23	0.844	0.207	22.22	0.759	0.257	29.40	0.901	0.245
3D-GS		28.69	0.870	0.182	23.14	0.841	0.183	29.41	0.903	0.243
Mip-Splatting		29.12	0.869	0.184	23.79	0.848	0.176	29.57	0.900	0.245
Scaffold-GS		29.35	0.870	0.188	24.14	0.853	0.175	30.26	0.909	0.252
PEP-GS (Ours)		29.80	0.870	0.183	24.79	0.862	0.163	30.00	0.910	0.249

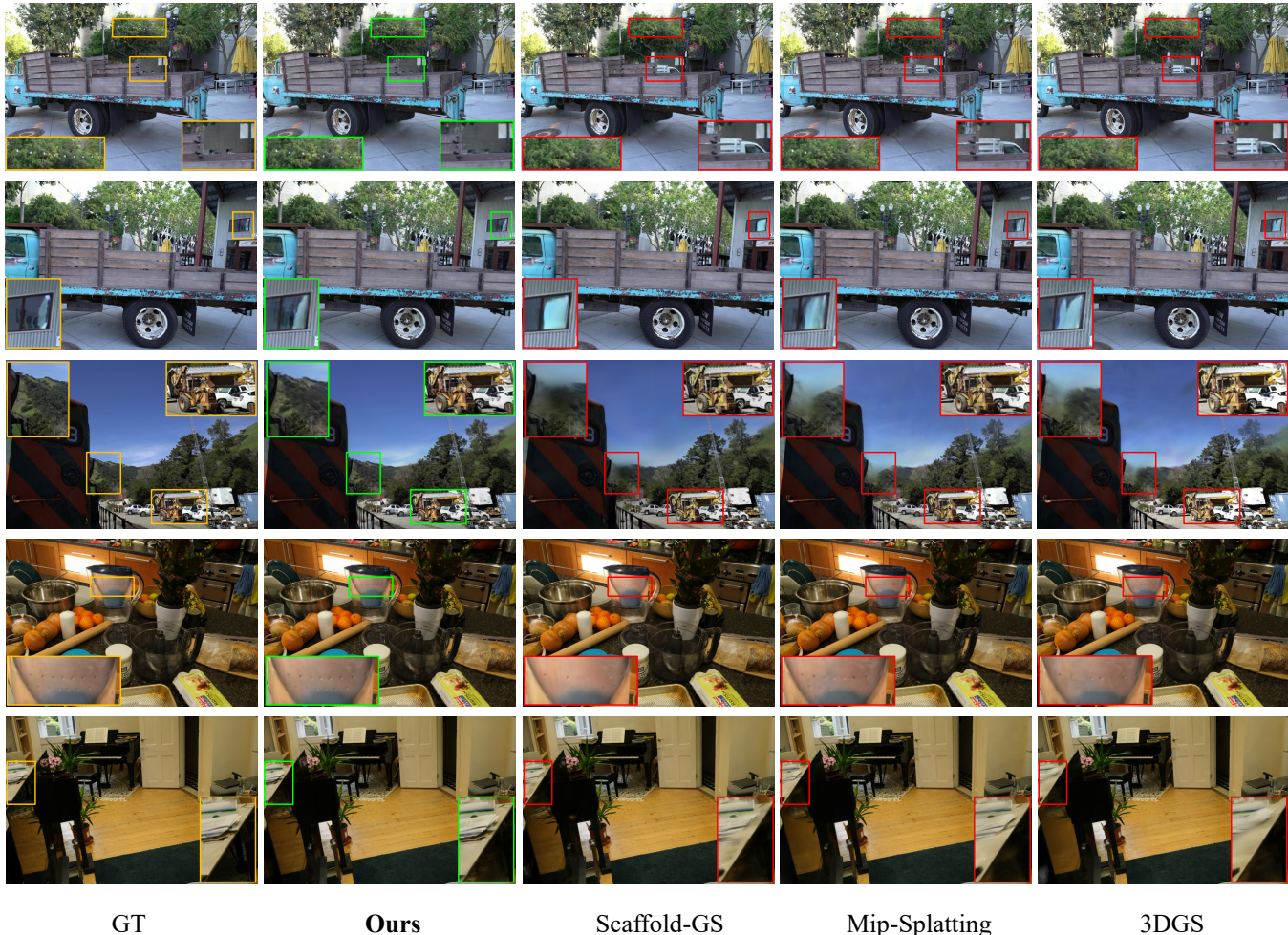


Figure 4: Compared to existing baselines, our method demonstrates superior detail preservation, reduced artifacts, and improved color consistency. Notably, in the second row of the images, our method also shows certain improvements in handling specular reflections compared to other approaches.

the Scaffold-GS method exhibits slightly excessive brightness, leading to the loss of certain details. In contrast, our method not only accurately maintains clearer textures and structural features but also avoids overexposure or shadow detail loss. Figure. 1 further illustrate that in challenging scenes like grass fields, our method better suppresses artifacts and unnatural textures while adeptly capturing complex textures and thin structures, exhibiting greater robustness. In terms of metric analysis, our method achieves lower LPIPS values and

higher SSIM scores, confirming its significant advantage in overall visual quality and perceptual consistency.

### 4.3 Ablation Study

To assess the effectiveness of each component of PEP-GS, we conducted ablation studies on the *room* scene from the Mip-NeRF360 dataset and the *truck* scene from the Tanks&Templates dataset. The quantitative and qualitative results are reported in Table. 2 and Figure. 5, respectively. We

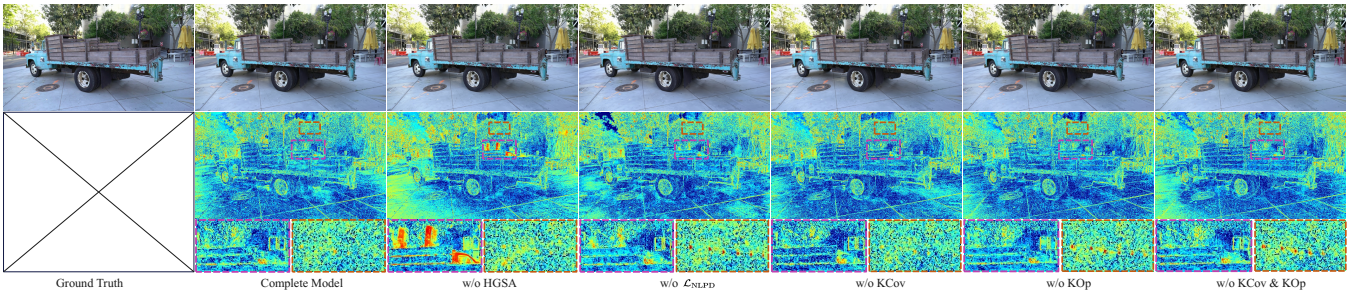


Figure 5: Ablation studies. The top images show our rendering results, and the bottom images present the error maps computed between these renderings and the ground truth (GT). In these maps, more intense colors denote larger discrepancies from the GT. Similar to Table. 2, KOp and KCov represent two methods that utilize the KAN framework to predict Gaussian opacity and covariance attributes, respectively.

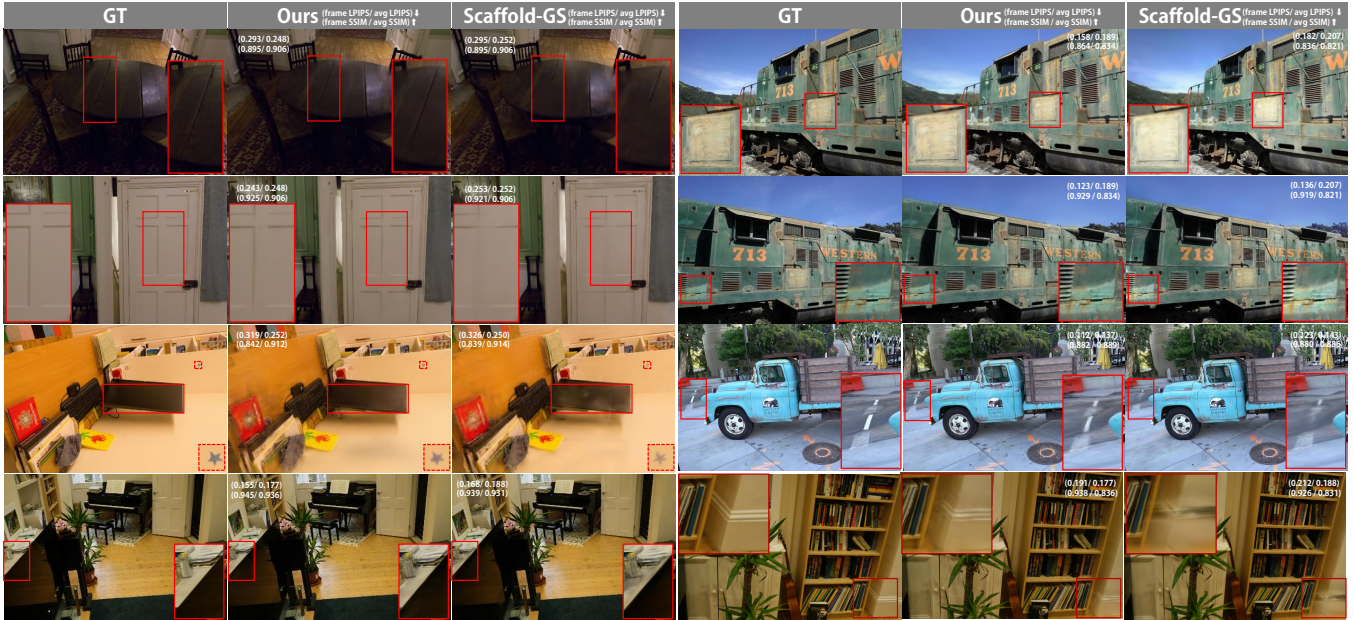


Figure 6: A systematic qualitative comparison between Scaffold-GS and PEP-GS is carried out across the Mip-NeRF360, Tanks&Temples, and Deep Blending datasets to highlight their relative strengths in diverse real-world scenarios.

Table 2: An ablation study evaluates the impact of removing components from PEP-GS.

Model setting	PSNR $\uparrow$	SSIM $\uparrow$	LPIPS $\downarrow$
1) w/o $\mathcal{L}_{NLPD}$	32.60	0.935	0.184
2) w/o HGSA	32.14	0.934	0.179
3) w/o KCov	33.10	0.936	0.178
4) w/o KOp	33.13	0.936	0.179
5) w/o both 3) and 4)	32.99	0.935	0.180
Our Complete Model	<b>33.19</b>	<b>0.936</b>	<b>0.177</b>

summarize our findings here.

**HGSA.** The removal of HGSA results in a marked degradation in both quantitative metrics and perceptual quality. As shown in Figure. 5, the rendered images result in false geometry without HGSA, introducing visual artifacts that were not present in the original scene. This degradation underscores the importance of HGSA in effectively capturing local geometric features and view-dependent effects. Its absence highlights the challenges of modeling intricate view-dependent

phenomena in 3D scenes.

**KCov&KOp.** The exclusion of either KCov or KOp alone leads to marginal decreases in performance metrics. However, removing both components results in a significant reduction in rendering quality. More importantly, the rendered images lack critical fine-grained details and exhibit poor representation of thin and delicate structures, such as small light bulbs or intricate textures. KCov and KOp collectively enhance the model’s ability to predict Gaussian attributes dynamically and precisely. These components ensure adaptive scaling and spatially consistent rendering, enabling the system to faithfully represent subtle geometric features and avoid over-simplification of the scene.

**$\mathcal{L}_{NLPD}$ .** Excluding  $\mathcal{L}_{NLPD}$  results in perceptual inconsistencies similar to those observed when KCov and KOp are removed. The absence of this multi-scale perceptual loss disrupts the model’s ability to align visual features across different spatial resolutions, leading to the loss of fine-scale details and textures, such as thin structures and small objects.  $\mathcal{L}_{NLPD}$  plays a critical role in ensuring the fidelity of recon-

structured textures and preserving structural details, particularly in scenes with complex geometric and photometric properties.

## 5 Conclusion and Limitation

In this paper, we propose PEP-GS, a perceptually-enhanced framework for structured 3D Gaussian splatting, addressing key challenges in view-adaptive rendering. Our method introduces a Hierarchical Granular-Structural Attention mechanism to better capture complex view-dependent effects, and utilizes Kolmogorov-Arnold Networks for robust and interpretable Gaussian attribute estimation. Additionally, the incorporation of the Normalized Laplacian Pyramid Distance loss enhances perceptual consistency across views, ensuring high-quality renderings with superior texture fidelity and geometric precision.

Even though experimental results show that PEP-GS surpasses existing methods, excelling in handling complex lighting and fine-scale details, there are still some limitations. Compared with scaffold-GS, while our method achieves superior metric scores and rendering performance, it slightly compromises rendering efficiency. We anticipate that our algorithm will progressively improve its rendering speed as the field advances.

## 6 Acknowledgments

This work is supported by the Hainan Provincial Natural Science Foundation of China (Grant No. 722RC678).

## References

- [Barron *et al.*, 2022] Jonathan T Barron, Ben Mildenhall, Dor Verbin, Pratul P Srinivasan, and Peter Hedman. Mip-nerf 360: Unbounded anti-aliased neural radiance fields. In *Proceedings of the IEEE/CVF Conference on Computer Vision and Pattern Recognition*, pages 5460–5469, 2022.
- [Barron *et al.*, 2023] Jonathan T. Barron, Ben Mildenhall, Dor Verbin, Pratul P. Srinivasan, and Peter Hedman. Zip-nerf: Anti-aliased grid-based neural radiance fields. In *Proceedings of the IEEE/CVF International Conference on Computer Vision (ICCV)*, pages 19697–19705, October 2023.
- [Botsch *et al.*, 2005] Mario Botsch, Alexander Hornung, Matthias Zwicker, and Leif Kobbelt. High-quality surface splatting on today’s gpus. In *Proceedings Eurographics/IEEE VGTC Symposium Point-Based Graphics, 2005.*, pages 17–141. IEEE, 2005.
- [Cao *et al.*, 2023] Junli Cao, Huan Wang, Pavlo Chemerys, Vladislav Shakhrai, Ju Hu, Yun Fu, Denys Makoviichuk, Sergey Tulyakov, and Jian Ren. Real-time neural light field on mobile devices. In *Proceedings of the IEEE/CVF Conference on Computer Vision and Pattern Recognition*, pages 8328–8337, 2023.
- [Chen *et al.*, 2022] Anpei Chen, Zexiang Xu, Andreas Geiger, Jingyi Yu, and Hao Su. Tensorf: Tensorial radiance fields. In *European conference on computer vision*, pages 333–350. Springer, 2022.
- [Chen *et al.*, 2023] Zhiqin Chen, Thomas Funkhouser, Peter Hedman, and Andrea Tagliasacchi. Mobilenerf: Exploiting the polygon rasterization pipeline for efficient neural field rendering on mobile architectures. In *Proceedings of the IEEE/CVF Conference on Computer Vision and Pattern Recognition*, pages 16569–16578, 2023.
- [Franke *et al.*, 2023] Linus Franke, Darius Rückert, Laura Fink, Matthias Innmann, and Marc Stamminger. Vet: Visual error tomography for point cloud completion and high-quality neural rendering. In *SIGGRAPH Asia 2023 Conference Papers*, pages 1–12, 2023.
- [Franke *et al.*, 2024] Linus Franke, Darius Rückert, Laura Fink, and Marc Stamminger. Trips: Trilinear point splatting for real-time radiance field rendering. In *Computer Graphics Forum*, page e15012. Wiley Online Library, 2024.
- [Fridovich-Keil *et al.*, 2022] Sara Fridovich-Keil, Alex Yu, Matthew Tancik, Qinhong Chen, Benjamin Recht, and Angjoo Kanazawa. Plenoxels: Radiance fields without neural networks. In *Proceedings of the IEEE/CVF Conference on Computer Vision and Pattern Recognition*, pages 5501–5510, 2022.
- [Hedman *et al.*, 2018] Peter Hedman, Julien Philip, True Price, Jan-Michael Frahm, George Drettakis, and Gabriel Brostow. Deep blending for free-viewpoint image-based rendering. *ACM Transactions on Graphics (ToG)*, 37(6):1–15, 2018.

- [Jiang *et al.*, 2024a] Ying Jiang, Chang Yu, Tianyi Xie, Xuan Li, Yutao Feng, Huamin Wang, Minchen Li, Henry Lau, Feng Gao, Yin Yang, et al. Vr-gs: A physical dynamics-aware interactive gaussian splatting system in virtual reality. In *ACM SIGGRAPH 2024 Conference Papers*, pages 1–1, 2024.
- [Jiang *et al.*, 2024b] Ying Jiang, Chang Yu, Tianyi Xie, Xuan Li, Yutao Feng, Huamin Wang, Minchen Li, Henry Lau, Feng Gao, Yin Yang, and Chenfanfu Jiang. Vr-gs: A physical dynamics-aware interactive gaussian splatting system in virtual reality. In *ACM SIGGRAPH 2024 Conference Papers*, SIGGRAPH '24, New York, NY, USA, 2024. Association for Computing Machinery.
- [Kerbl *et al.*, 2023] Bernhard Kerbl, Georgios Kopanas, Thomas Leimkühler, and George Drettakis. 3d gaussian splatting for real-time radiance field rendering. *ACM Transactions on Graphics*, 42(4), July 2023.
- [Knapitsch *et al.*, 2017] Arno Knapitsch, Jaesik Park, Qian-Yi Zhou, and Vladlen Koltun. Tanks and temples: Benchmarking large-scale scene reconstruction. *ACM Transactions on Graphics*, 36(4), 2017.
- [Kopanas *et al.*, 2021] Georgios Kopanas, Julien Philip, Thomas Leimkühler, and George Drettakis. Point-based neural rendering with per-view optimization. In *Computer Graphics Forum*, volume 40, pages 29–43. Wiley Online Library, 2021.
- [Laparra *et al.*, 2016] Valero Laparra, Johannes Ballé, Alexander Bernardino, and Eero P Simoncelli. Perceptual image quality assessment using a normalized laplacian pyramid. *Electronic Imaging*, 28:1–6, 2016.
- [Liu *et al.*, 2024] Ziming Liu, Yixuan Wang, Sachin Vaidya, Fabian Rühle, James Halverson, Marin Soljačić, Thomas Y Hou, and Max Tegmark. Kan: Kolmogorov-arnold networks. *arXiv preprint arXiv:2404.19756*, 2024.
- [Lu *et al.*, 2024] Tao Lu, Mulin Yu, Linning Xu, Yuanbo Xiangli, Limin Wang, Dahua Lin, and Bo Dai. Scaffoldgs: Structured 3d gaussians for view-adaptive rendering. In *Proceedings of the IEEE/CVF Conference on Computer Vision and Pattern Recognition*, pages 20654–20664, 2024.
- [Ma *et al.*, 2024] Li Ma, Vasu Agrawal, Haithem Turki, Changil Kim, Chen Gao, Pedro Sander, Michael Zollhöfer, and Christian Richardt. Specnerf: Gaussian directional encoding for specular reflections. In *Proceedings of the IEEE/CVF Conference on Computer Vision and Pattern Recognition*, pages 21188–21198, 2024.
- [Mildenhall *et al.*, 2021] Ben Mildenhall, Pratul P Srinivasan, Matthew Tancik, Jonathan T Barron, Ravi Ramamoorthi, and Ren Ng. Nerf: Representing scenes as neural radiance fields for view synthesis. *Communications of the ACM*, 65(1):99–106, 2021.
- [Müller *et al.*, 2022] Thomas Müller, Alex Evans, Christoph Schied, and Alexander Keller. Instant neural graphics primitives with a multiresolution hash encoding. *ACM Transactions on Graphics*, 41(4):1–15, 2022.
- [Munkberg *et al.*, 2022] Jacob Munkberg, Jon Hasselgren, Tianchang Shen, Jun Gao, Wenzheng Chen, Alex Evans, Thomas Müller, and Sanja Fidler. Extracting triangular 3d models, materials, and lighting from images. In *Proceedings of the IEEE/CVF Conference on Computer Vision and Pattern Recognition*, pages 8280–8290, 2022.
- [Qian *et al.*, 2024a] Shenhan Qian, Tobias Kirschstein, Liam Schoneveld, Davide Davoli, Simon Giebenhain, and Matthias Nießner. Gaussianavatars: Photorealistic head avatars with rigged 3d gaussians. In *Proceedings of the IEEE/CVF Conference on Computer Vision and Pattern Recognition*, pages 20299–20309, 2024.
- [Qian *et al.*, 2024b] Zhiyin Qian, Shaofei Wang, Marko Mihajlovic, Andreas Geiger, and Siyu Tang. 3dgs-avatar: Animatable avatars via deformable 3d gaussian splatting. In *Proceedings of the IEEE/CVF Conference on Computer Vision and Pattern Recognition*, pages 5020–5030, 2024.
- [Reiser *et al.*, 2021] Christian Reiser, Songyou Peng, Yiyi Liao, and Andreas Geiger. Kilonerf: Speeding up neural radiance fields with thousands of tiny mlps. In *Proceedings of the IEEE/CVF international conference on computer vision*, pages 14335–14345, 2021.
- [Reiser *et al.*, 2023] Christian Reiser, Rick Szeliski, Dor Verbin, Pratul Srinivasan, Ben Mildenhall, Andreas Geiger, Jon Barron, and Peter Hedman. Merf: Memory-efficient radiance fields for real-time view synthesis in unbounded scenes. *ACM Transactions on Graphics (TOG)*, 42(4):1–12, 2023.
- [Sitzmann *et al.*, 2021] Vincent Sitzmann, Semon Reizchikov, Bill Freeman, Josh Tenenbaum, and Fredo Durand. Light field networks: Neural scene representations with single-evaluation rendering. *Advances in Neural Information Processing Systems*, 34:19313–19325, 2021.
- [Snively *et al.*, 2023] Noah Snively, Steven M. Seitz, and Richard Szeliski. *Photo Tourism: Exploring Photo Collections in 3D*. Association for Computing Machinery, New York, NY, USA, 1 edition, 2023.
- [Verbin *et al.*, 2022] Dor Verbin, Peter Hedman, Ben Mildenhall, Todd Zickler, Jonathan T Barron, and Pratul P Srinivasan. Ref-nerf: Structured view-dependent appearance for neural radiance fields. In *2022 IEEE/CVF Conference on Computer Vision and Pattern Recognition (CVPR)*, pages 5481–5490. IEEE, 2022.
- [Wang *et al.*, 2004] Zhou Wang, A.C. Bovik, H.R. Sheikh, and E.P. Simoncelli. Image quality assessment: from error visibility to structural similarity. *IEEE Transactions on Image Processing*, 13(4):600–612, 2004.
- [Xie *et al.*, 2024] Tianyi Xie, Zeshun Zong, Yuxing Qiu, Xuan Li, Yutao Feng, Yin Yang, and Chenfanfu Jiang. Physgaussian: Physics-integrated 3d gaussians for generative dynamics. In *Proceedings of the IEEE/CVF Conference on Computer Vision and Pattern Recognition*, pages 4389–4398, 2024.
- [Xu and Wan, 2024] Wei Xu and Yi Wan. Ela: Efficient local attention for deep convolutional neural networks. *arXiv preprint arXiv:2403.01123*, 2024.

- [Xu *et al.*, 2022] Qiangeng Xu, Zexiang Xu, Julien Philip, Sai Bi, Zhixin Shu, Kalyan Sunkavalli, and Ulrich Neumann. Point-nerf: Point-based neural radiance fields. In *Proceedings of the IEEE/CVF Conference on Computer Vision and Pattern Recognition*, pages 5438–5448, 2022.
- [Xu *et al.*, 2023] Linning Xu, Vasu Agrawal, William Laney, Tony Garcia, Aayush Bansal, Changil Kim, Samuel Rota Bulò, Lorenzo Porzi, Peter Kotschieder, Aljaž Božič, et al. Vr-nerf: High-fidelity virtualized walkable spaces. In *SIGGRAPH Asia 2023 Conference Papers*, pages 1–12, 2023.
- [Yang *et al.*, 2024] Ziyi Yang, Xinyu Gao, Yangtian Sun, Yihua Huang, Xiaoyang Lyu, Wen Zhou, Shaohui Jiao, Xiaojuan Qi, and Xiaogang Jin. Spec-gaussian: Anisotropic view-dependent appearance for 3d gaussian splatting. *arXiv preprint arXiv:2402.15870*, 2024.
- [Yifan *et al.*, 2019] Wang Yifan, Felice Serena, Shihao Wu, Cengiz Öztireli, and Olga Sorkine-Hornung. Differentiable surface splatting for point-based geometry processing. *ACM Transactions on Graphics (TOG)*, 38(6):1–14, 2019.
- [Yu *et al.*, 2023] Zehao Yu, Anpei Chen, Binbin Huang, Torsten Sattler, and Andreas Geiger. Mip-splatting: Alias-free 3d gaussian splatting. *arXiv preprint arXiv:2311.16493*, 2023.
- [Zhang *et al.*, 2018] Richard Zhang, Phillip Isola, Alexei A Efros, Eli Shechtman, and Oliver Wang. The unreasonable effectiveness of deep features as a perceptual metric. In *Proceedings of the IEEE conference on computer vision and pattern recognition*, pages 586–595, 2018.
- [Zheng *et al.*, 2024] Shunyuan Zheng, Boyao Zhou, Ruizhi Shao, Boning Liu, Shengping Zhang, Liqiang Nie, and Yebin Liu. Gps-gaussian: Generalizable pixel-wise 3d gaussian splatting for real-time human novel view synthesis. In *Proceedings of the IEEE/CVF Conference on Computer Vision and Pattern Recognition*, pages 19680–19690, 2024.
- [Zhou *et al.*, 2024] Xiaoyu Zhou, Zhiwei Lin, Xiaojun Shan, Yongtao Wang, Deqing Sun, and Ming-Hsuan Yang. Drivinggaussian: Composite gaussian splatting for surrounding dynamic autonomous driving scenes. In *Proceedings of the IEEE/CVF Conference on Computer Vision and Pattern Recognition (CVPR)*, pages 21634–21643, June 2024.

## Appendix

We present comprehensive evaluation metrics for all scenes from the three public datasets mentioned in the main text. As shown in Tables. 3 and 4, our model consistently achieves superior performance across the majority of scenes. These quantitative results align with the enhanced perceptual capabilities of our model, further illustrated in Figures. ?? and 7.

In indoor scenes such as Playroom and Dr Johnson, our method excels in handling complex lighting conditions and preserving fine geometric details, areas where traditional methods often struggle. The integration of our Hierarchical Granular-Structural Attention (HGSA) mechanism plays a crucial role in maintaining consistency across different viewing angles while effectively preserving intricate texture details.

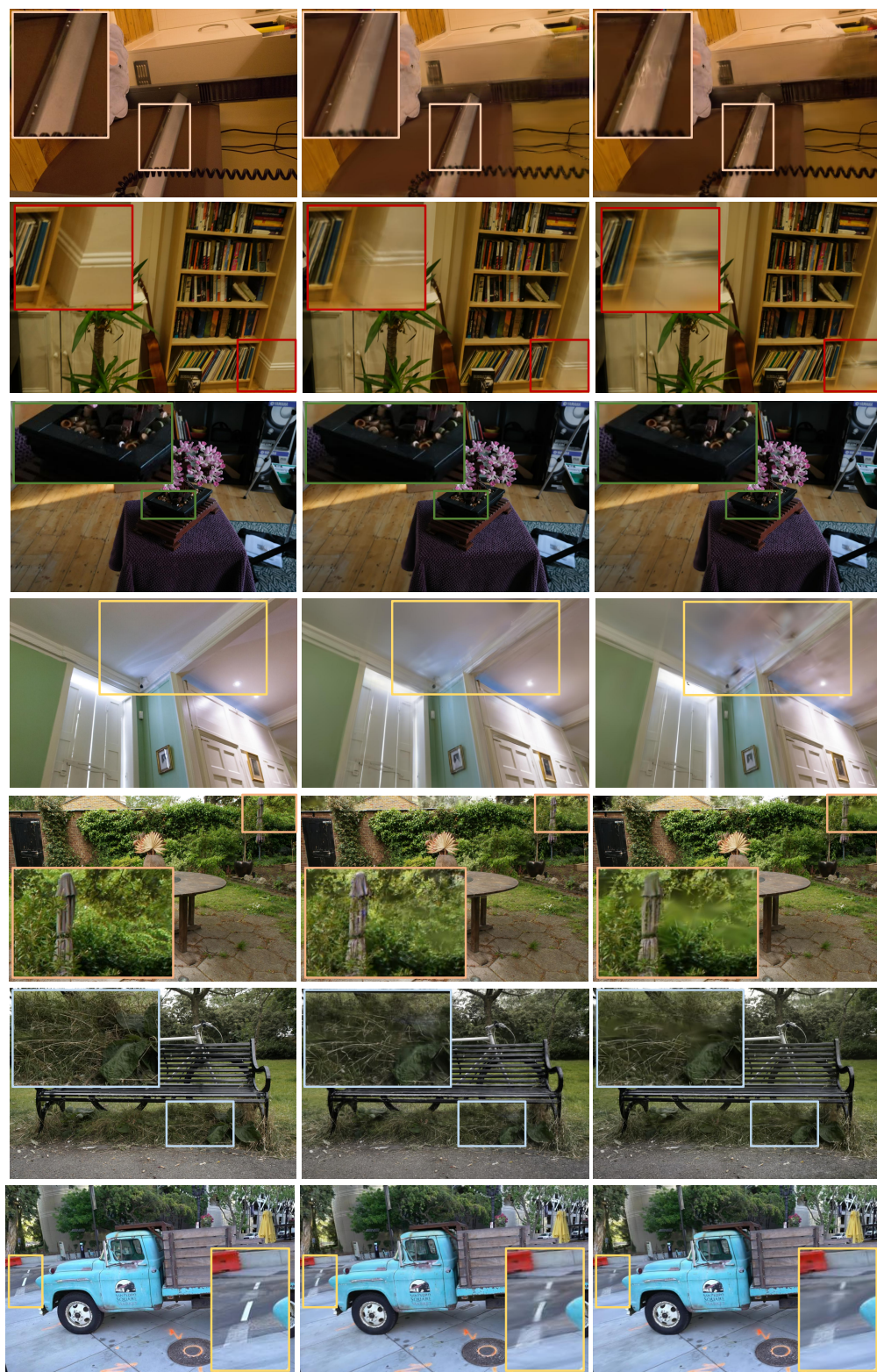
Similarly, in outdoor environments like Truck and Garden, our approach demonstrates a remarkable capability in managing natural lighting variations and capturing complex geometric structures with high fidelity. The effectiveness of our Kolmogorov-Arnold Networks (KAN) for opacity and covariance estimation is particularly evident in challenging scenarios involving thin structures and texture-less regions. This component ensures precise control over Gaussian attributes, leading to more accurate geometric reconstruction and improved preservation of fine-scale details.

Table 3: Quantitative performance comparison across Tanks&Temples and Deep Blending scenes.

		PSNR↑			
Method	Scenes	Truck	Train	Dr Johnson	Playroom
Instant-NGP		23.26	20.17	27.75	19.48
Plenoxels		23.22	18.93	23.14	22.98
Mip-NeRF360		24.91	19.52	29.14	29.66
3D-GS		25.19	21.10	28.77	30.04
Mip-Splatting		25.56	22.02	29.11	30.03
Scaffold-GS		25.82	22.46	<b>29.68</b>	<b>30.84</b>
PEP-GS (Ours)		<b>26.34</b>	<b>23.24</b>	29.33	30.66
		SSIM↑			
Method	Scenes	Truck	Train	Dr Johnson	Playroom
Instant-NGP		0.779	0.666	0.899	0.906
Plenoxels		0.774	0.663	0.787	0.802
Mip-NeRF360		0.857	0.660	0.901	0.900
3D-GS		0.879	0.802	0.899	0.906
Mip-Splatting		0.881	0.816	0.899	0.902
Scaffold-GS		0.886	0.821	<b>0.906</b>	0.912
PEP-GS (Ours)		<b>0.889</b>	<b>0.834</b>	<b>0.906</b>	<b>0.914</b>
		LPIPS↓			
Method	Scenes	Truck	Train	Dr Johnson	Playroom
Instant-NGP		0.274	0.386	0.381	0.465
Plenoxels		0.335	0.422	0.521	0.499
Mip-NeRF360		0.159	0.354	<b>0.237</b>	0.252
3D-GS		0.148	0.218	0.244	<b>0.241</b>
Mip-Splatting		0.147	0.205	0.245	0.245
Scaffold-GS		0.143	0.207	0.252	0.252
PEP-GS (Ours)		<b>0.137</b>	<b>0.189</b>	0.248	0.250

Table 4: Quantitative performance comparison across Mip-NeRF 360 scenes.

		PSNR $\uparrow$						
Method	Scenes	Bicycle	Garden	Stump	Room	Counter	Kitchen	Bonsai
Instant-NGP		22.19	24.60	23.63	29.27	26.44	28.55	30.34
Plenoxels		21.91	23.49	20.66	27.59	23.62	23.42	24.67
Mip-NeRF360		24.37	26.98	26.40	31.63	29.55	<b>32.23</b>	33.46
3D-GS		<b>25.25</b>	27.41	26.55	30.63	28.70	30.32	31.98
Mip-Splatting		25.13	27.35	26.63	31.75	29.12	31.51	32.36
Scaffold-GS		25.20	27.28	26.63	32.15	29.66	31.77	32.78
PEP-GS (Ours)		25.11	<b>27.61</b>	<b>26.66</b>	<b>33.19</b>	<b>30.26</b>	31.87	<b>33.93</b>
		SSIM $\uparrow$						
Method	Scenes	Bicycle	Garden	Stump	Room	Counter	Kitchen	Bonsai
Instant-NGP		0.491	0.649	0.574	0.855	0.798	0.818	0.890
Plenoxels		0.496	0.606	0.523	0.842	0.759	0.648	0.814
Mip-NeRF360		0.685	0.813	0.744	0.913	0.894	0.920	0.941
3D-GS		<b>0.771</b>	<b>0.868</b>	<b>0.775</b>	0.914	0.905	0.922	0.938
Mip-Splatting		0.747	0.853	0.769	0.925	0.913	0.931	0.945
Scaffold-GS		0.746	0.850	0.765	0.931	<b>0.919</b>	0.932	0.949
PEP-GS (Ours)		0.735	0.852	0.758	<b>0.936</b>	<b>0.919</b>	<b>0.935</b>	<b>0.955</b>
		LPIPS $\downarrow$						
Method	Scenes	Bicycle	Garden	Stump	Room	Counter	Kitchen	Bonsai
Instant-NGP		0.487	0.312	0.450	0.301	0.342	0.254	0.227
Plenoxels		0.506	0.386	0.503	0.419	0.441	0.447	0.398
Mip-NeRF360		0.301	0.170	0.261	0.211	0.204	0.127	0.176
3D-GS		<b>0.205</b>	<b>0.103</b>	<b>0.210</b>	0.220	0.204	0.129	0.205
Mip-Splatting		0.245	0.123	0.242	0.197	0.183	0.116	0.181
Scaffold-GS		0.256	0.135	0.259	0.188	0.181	0.118	0.178
PEP-GS (Ours)		0.260	0.130	0.257	<b>0.177</b>	<b>0.176</b>	<b>0.113</b>	<b>0.168</b>



Ground Truth

PEP-GS (Ours)

Scaffold-GS

Figure 7: Qualitative comparison between PEP-GS (Ours) and Scaffold-GS.